Letter

Emergent slow dynamics of collapsed polymers flowing through porous media

Hsieh Chen* and Martin E. Poitzsch
Aramco Services Company: Aramco Research Center-Boston, Cambridge, Massachusetts 02139, USA

(Received 11 November 2020; accepted 8 April 2021; published 28 April 2021)

Using hydrodynamic simulations, we study the single polymers flowing through model porous media (close-packed colloidal crystal). In good solvent or high flow rates, the polymer transport is similar to gel electrophoresis, with size-dependent sieving for $L_c/L \lesssim 1$ and size-independent biased reptation for $L_c/L \gtrsim 1$ (L_c is the polymer contour length and L is the diameter of colloids forming the porous media). Importantly, in bad solvent and low flow rates, the polymers show an extra window of size-dependent velocity for $1 \lesssim L_c/L \lesssim 2$, where the polymer transport is controlled by a globule-stretch transition at pore throats, and the transport velocity is much slower than reptation.

DOI: 10.1103/PhysRevE.103.L040501

Understanding the transport of polymers in porous media is important in many industrial and technological applications. In biotechnology, the polymer transport in porous media has been discussed in the framework of DNA separation. The objective is to effectively separate DNAs (or other biomacromolecules) according to their sizes. In traditional DC gel electrophoresis, size-dependent Ogston sieving is the main separation mechanism for short DNAs until the DNA sizes become larger than the gel pores, where size-independent *biased reptation* dynamics (i.e., biased diffusion of long-chain molecules along confined random path of tubes towards the direction of applied electric field) starts to dominate [1]. To overcome this, different microfluidic devices have been designed for the separation of larger DNA molecules beyond gel electrophoresis [2,3].

Industrially, large amounts of polymers have been injected into subsurface rock matrices for enhanced oil recovery and groundwater remediation applications [4,5]. The effectiveness of these projects ties greatly to the successful transport of polymers while maintaining the polymers' rheological properties. When the polymer sizes are smaller than the rock pores, the polymers are lost in the rock matrices mainly through chemical adsorptions. However, when polymer sizes are commensurate with rock pores, mechanical entrapments may play a dominant role that hinders the polymer transport [6–8]. Despite the direct relevance in successful polymer flooding, a clear physical picture for polymer mechanical entrapments in porous media is still surprisingly lacking.

Microfluidic experiments have been invaluable in visualizing the polymer dynamics when flowing through porous media; however, due to fabrication limitations, they have mainly focused on 2D geometries, even though the pore space in a 2D medium is considerably less connected and tortuous than 3D [9–13]. On the other hand, molecular simulations have been used to further the understanding of polymer transport in porous media (or arrays of obstacles). Nevertheless, most of the simulation works have been carried out in the context of DNA electrophoresis that the polymers were driven by electrical fields, whereas the flow-driven dynamics were less explored [14–17].

Finally, it has been identified that solvent properties may have pronounced effects for polymer dynamics, especially under nonequilibrium conditions [18–21]. In this paper, we study the transport of polymers through model 3D porous media driven by fluid flows under different flow rates and solvent properties using molecular simulations with fully coupled hydrodynamic interactions. As we will show, for collapsed polymers (i.e., polymers in bad solvent) flowing through porous media, there can emerge a slow dynamics that the polymer transport is controlled by a *globule-stretch transition* at the pore throats and the transport velocity is much slower than the noncollapsed polymers, which, to the best of our knowledge, has not been reported. (Note the globule-stretch transition refers to the abrupt unwinding of cohesive globular polymers under strong flows that is triggered by an instability on the globular polymer surfaces [18,20,22].) This finding is important for understanding the mechanical entrapment when using polymers for subsurface applications (where the high temperature and high salinity subsurface environments can push the polymers to the more collapsed state), and to design alternative mechanisms for the separations of (bio)macromolecules.

For (bio)macromolecular separations and polymer subsurface applications, the polymer and porous media length scales can have wide variations [1–5]. The polymer counter lengths (L_c) can range from ∼100 nm for small proteins and synthetic polymers to ∼10 μm for double-stranded DNAs and other biopolymers such as xanthan. On the other hand, the porous media pore–grain sizes (L) can range from ∼100 nm for agarose gel and tight formation rocks to ∼10 μm for microfluidic devices and unconsolidated sand packs. In this work, we have focused on $L_c/L \sim O(1)$ that has the richest polymer-porous media interactions since for $L_c/L \ll 1$ the polymers may be approximated as free-flowing without confinements, and for $L_c/L \gg 1$ the polymers may

*hsieh.chen@aramcoamericas.com

predominately be jammed at the entrance of the porous media or bypass the porous media entirely. In addition to the length scales, the kinematic parameters can have wide variations as well [11,23,24], with the fluid velocity within the pores $V_p \sim 10^{-2}$ to 10^2 μm/s, fluid viscosity $\eta \sim 1$ to 100 cP, and temperature $T \sim 298$ to 373 K. The ranges of the Reynolds number and Péclet number are $Re = \rho V_p L/\eta \sim 10^{-11}$ to 10^{-3} and $Pe = V_p L/D \sim V_p L/(k_B T/6\pi\eta L_c) \sim 1$ to 10^{10}, respectively.

We model the homopolymer by N freely jointed beads of radius a interacting through the intrinsic potential $U = U_s + U_{LJ}$. The first term accounts for the connectivity of the chain, $U_s = \frac{\kappa}{2} k_B T \sum_{i=1}^{N-1} (r_{i+1,i} - 2a)^2$, where $r_{i+1,i}$ is the distance between adjacent beads along the chain, and the spring constant is taken to be $\kappa = 500/a^2$ that limits stretching of the chain [25,26]. The second term is a Lennard-Jones potential $U_{LJ} = \varepsilon k_B T \sum_{ij}[(2a/r_{i,j})^{12} - 2(2a/r_{i,j})^6]$, where ε determines the depth of the potential, and $r_{i,j}$ is the distance between the ith and the jth bead. Note in polymer physics literature the solvent properties have been referred to as *good* and *bad (or poor) solvents* [27]. For a good solvent, interactions between polymer segments and solvent molecules are energetically favorable and will cause polymer chains to expand. For a bad solvent, polymer-polymer self-interactions are preferred, and the polymer chains will collapse. In this work, we use a good solvent for which $\varepsilon = 0.41$ and a bad solvent with $\varepsilon = 2.08$ that strongly collapses the chains [20]. The model 3D porous media is made with face-centered-cubic (fcc) close-packed colloidal crystal with diameter L where polymers can travel within the pore spaces (Fig. 1, inset). Chemical adsorption is not considered in this work and purely repulsive forces are used between polymers and colloids to which a stiff Hookean interaction is applied if the distance between the monomers and colloids is less than the sum of their radii. The hydrodynamics in the pore spaces is modeled by the fluctuating lattice-Boltzmann (LB) equation [28], with the link bounce-back boundary conditions on the surfaces of the colloids [29]. For simplicity, we set the LB grid spacing Δx and time step Δt equal to unity. Other parameters for the fluid are the density $\rho = 1$, the kinematic viscosity $\nu = 1/6$, and the temperature $k_B T = 1 \times 10^{-4}$ to 2×10^{-4} (normalized to the lattice units ρ, Δx, and Δt; see Refs. [28,30] for the details of choosing simulation parameters). The polymer beads couple to the fluid in a dissipative manner [31,32], from friction forces based on the differences between the velocities of the monomers $\mathbf{u}_i$ and the fluid velocities $\mathbf{u}_{LB}$ (interpolated at the monomer positions), $\mathbf{F}_{fl} = -\xi(\mathbf{u}_i - \mathbf{u}_{LB}) + \mathbf{R}_i$, where ξ is a friction constant and $\mathbf{R}_i$ is a random force of local covariance $\langle \mathbf{R}_i(t)\mathbf{R}_j(t')\rangle = 2k_B T\xi\delta(t-t')\delta_{ij}\mathbf{I}$ introduced to balance the additional dissipation. The equations of motion for the ith monomer are then $\frac{d\mathbf{r}_i}{dt} = \mathbf{u}_i$ and $m\frac{d\mathbf{u}_i}{dt} = \mathbf{F}_{fl} - \nabla U_i$. Finally, the opposite forces $-\mathbf{F}_{fl}$ are applied back to the fluid to conserve the total momentum. In the LB unit, the effective radius of the polymer beads is $a = 0.5$, and the characteristic monomer diffusion time is $\tau = 6\pi\eta a^3/k_B T = 2 \times 10^3$ to 4×10^3, where η is the dynamic viscosity of the fluid that $\eta = \nu\rho$. Similar approach has been used to study the dynamics of polymer-colloid mixtures in flow [25,26,33,34]. The simulation box consists of a fcc colloidal crystal unit cell with edge length $= 51$, and the diameter of the colloids is $L = 18$. To control the flow rates, different periodic pressure drops [35] are applied in the three dimensions that result in a net pore velocity in the $\langle 111\rangle$ direction with the average pore velocity strengths $V_p = 2.7 \times 10^{-4}$ to 5.3×10^{-5}. We mainly focus on the $\langle 111\rangle$ direction because it represents the most tortuous path within the fcc colloidal crystal [36]. Finally, the monomer Péclet number is defined as $Pe = V_p L/D = V_p L/(k_B T/6\pi\eta a) = 15$ to 150 and the Reynolds number is $Re = \rho V_p L/\eta \sim 10^{-3}$ to 10^{-2} in this work. Note both Pe and Re are within the reasonable ranges for the (bio)macromolecular separations and polymer subsurface applications as discussed above.

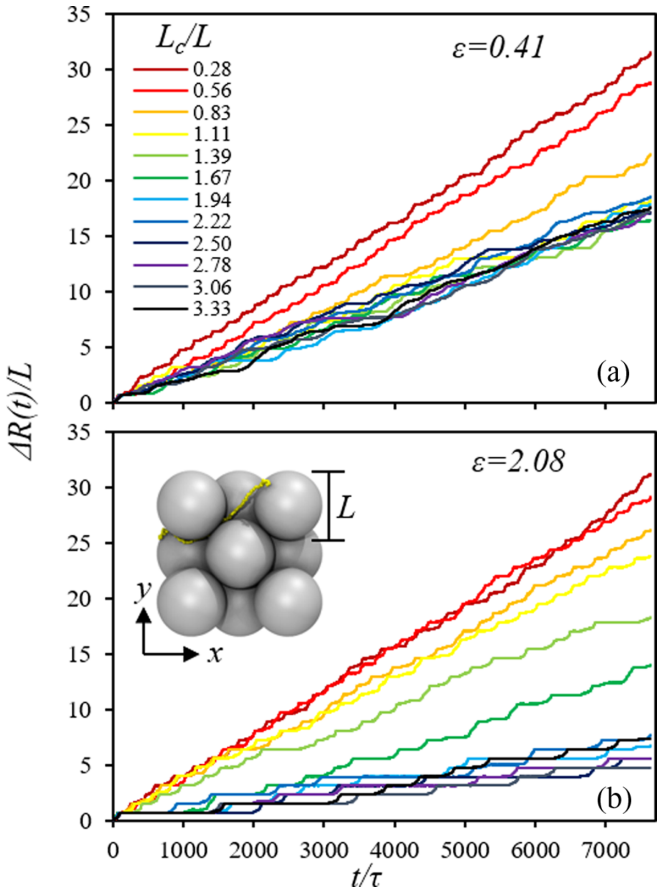

FIG. 1. Time sequences of the displacements of polymer center of mass along the flow direction $\Delta R(t)/L$ with different polymer lengths L_c/L in (a) good ($\varepsilon = 0.41$) or (b) bad solvents ($\varepsilon = 2.08$) for flow rate $Pe = 15$. Inset: representative simulation snapshot for a polymer flowing through model porous media (face-centered-cubic colloidal crystal).

Figure 1 shows the time sequences of the displacements of the polymer center of mass along the flow direction, $\Delta R(t)$, with different polymer contour lengths $L_c = 2Na$ for $N = 10$ to 120 ($L_c/L = 0.28$ to 3.33) in a good solvent [$\varepsilon = 0.41$, Fig. 1(a)] or in a bad solvent [$\varepsilon = 2.08$, Fig. 1(b)] for low flow rate ($Pe = 15$). As can be seen, in bad solvent the polymer displacements are greatly reduced for the longer chains with wider ranges of size-dependent spreads. Specifically, at the end of the simulations, in good solvent $\Delta R(t)/L$ decreases from ~30 to ~15 when L_c/L increases from 0.28 to 1.11 and

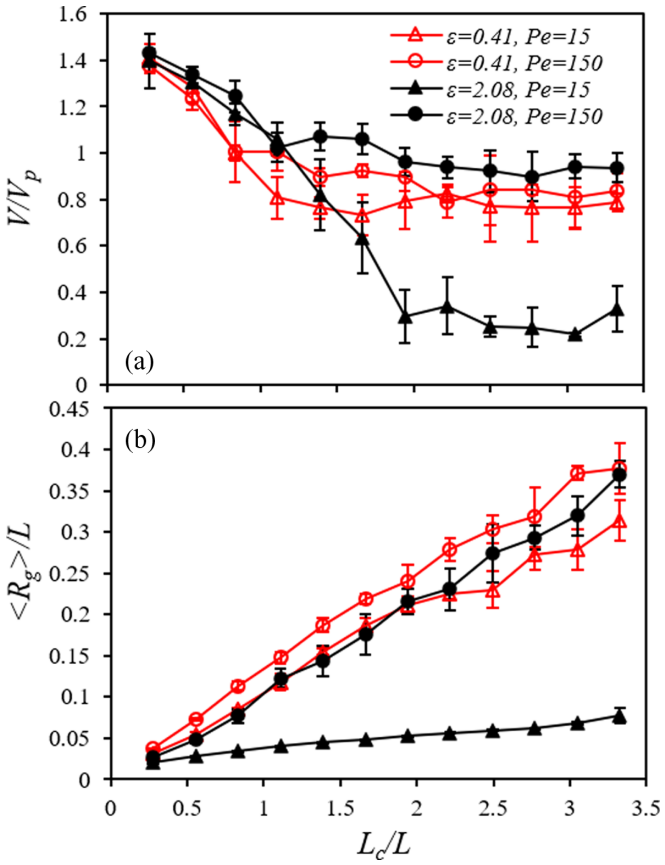

FIG. 2. (a) Ratios of polymer center of mass velocity and pore fluid velocity V/V_p, and (b) polymer radius of gyration $\langle R_g\rangle/L$ as a function of polymer lengths L_c/L at different flow rates and solvent properties. Note the error bars represent the standard deviations between block averages by separating the total simulation sequences into three or four segments (cf. Fig. 1).

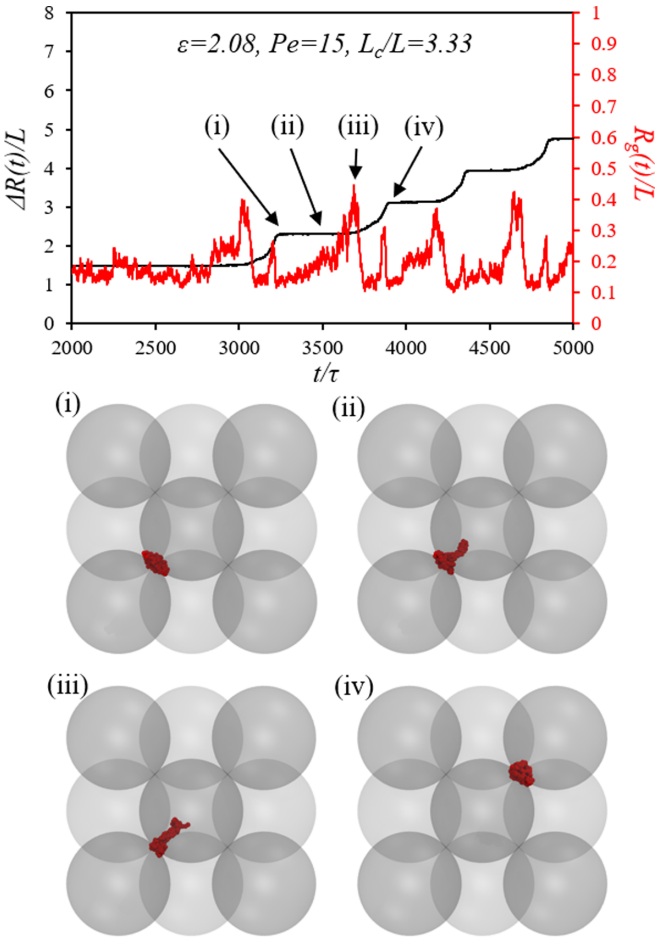

FIG. 3. Representative time sequences of the polymer displacement $\Delta R(t)/L$ and radius of gyration $R_g(t)/L$ for a long polymer ($L_c/L = 3.33$) passes through pore throats and representative simulation snapshots for the $\varepsilon = 2.08$, $Pe = 15$ case. In the snapshots, the porous media are drawn with transparent spheres, and the collapsed polymer is drawn with red beads.

stops changing when $L_c/L > 1.11$ [Fig. 1(a)]. In contrast, in bad solvent $\Delta R(t)/L$ keeps decreasing from ∼30 to ∼5 when L_c/L increases from 0.28 to 2.22 and stops changing only after $L_c/L > 2.22$ [Fig. 1(b)].

Figure 2(a) summarizes the ratios of polymer center of mass velocity and pore fluid velocity V/V_p driven by low ($Pe = 15$) or high flow rates ($Pe = 150$) in good ($\varepsilon = 0.41$) or bad solvent ($\varepsilon = 2.08$). The polymer velocity is calculated by $V = \Delta R(t)/t$, and the error bars represent the standard deviations between block averages by separating the total simulation sequences into 3 or 4 segments (cf. Fig. 1) [37]. As shown, for noncollapsed polymers in all flow rates ($\varepsilon = 0.41$, $Pe = 15$ or 150) and collapsed polymers in high flow rate ($\varepsilon = 2.08$, $Pe = 150$), V/V_p decreases from ∼1.4 to ∼0.8 or ∼1 for $L_c/L \lesssim 1$ and plateaus for $L_c/L \gtrsim 1$. The polymer transport velocities with size-dependent sieving for short chains and size-independent biased reptation for longer chains have been observed in the gel electrophoresis for DNA molecules driven by electrical fields [1,2]. Here, we show that similar dynamics can be observed for the polymers driven by fluid flows as well. Importantly, for collapsed polymers in low flow rate ($\varepsilon = 2.08$, $Pe = 15$), there emerges a very distinct dynamics that V/V_p keeps decreasing from ∼1.4 to ∼0.2 for $L_c/L \lesssim 2$ and then plateaus after $L_c/L \gtrsim 2$, with the polymer transport velocity much slower than the biased reptation. Figure 2(b) shows the polymer radius of gyration $\langle R_g\rangle$ in all simulation conditions. For noncollapsed polymers in all flow rates and collapsed polymers in high flow rate ($\varepsilon = 0.41$, $Pe = 15$ or 150; $\varepsilon = 2.08$, $Pe = 150$), $\langle R_g\rangle$ are comparable ($\langle R_g\rangle/L$ increases from ∼0.04 to ∼0.4 for L_c/L increases from 0.28 to 3.33), suggesting similarly chain-stretching dynamics when flowing through porous media. In contrast, for collapsed polymers in low flow rate ($\varepsilon = 2.08$, $Pe = 15$), $\langle R_g\rangle$ is much smaller ($\langle R_g\rangle/L < 0.1$ for all L_c/L) than the previous cases, suggesting different transport dynamics that the chains are in the collapsed state most of the time.

To gain further insight for the slowing dynamics of the collapsed polymers in low flow rate, Fig. 3 shows the representative time sequences of the polymer displacement $\Delta R(t)/L$ and radius of gyration $R_g(t)/L$ when a long polymer ($L_c/L = 3.33$) passes through pore throats as well as representative simulation snapshots for the $\varepsilon = 2.08$, $Pe = 15$ case. When first arriving at a pore throat, the polymer globule is larger than the pore throat and cannot pass through

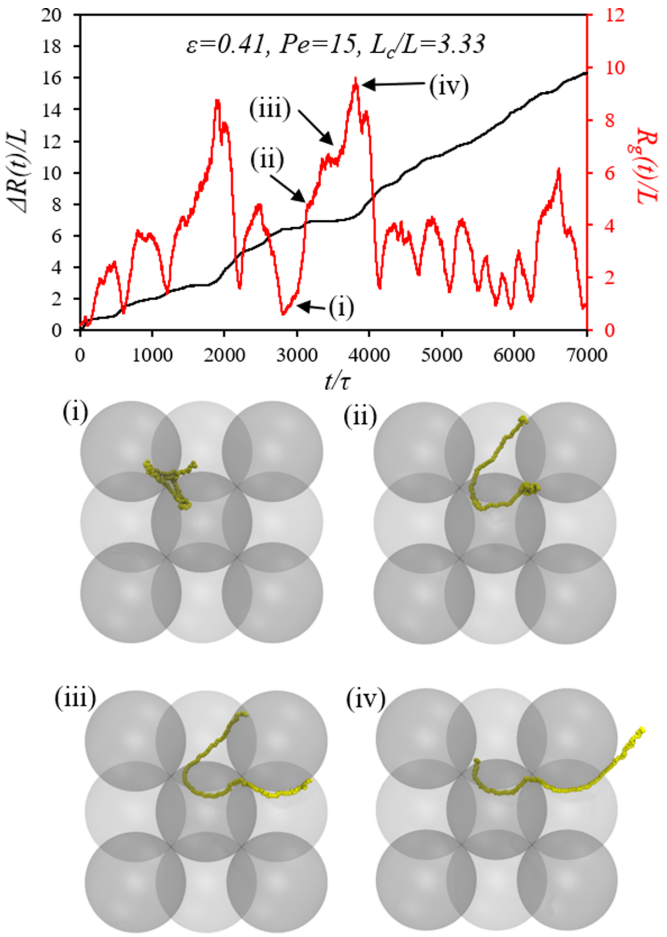

FIG. 4. Representative time sequences of the polymer displacement $\Delta R(t)/L$ and radius of gyration $R_g(t)/L$ for a long polymer ($L_c/L = 3.33$) passes through pore throats and representative simulation snapshots for the $\varepsilon = 0.41$, $Pe = 15$ case. In the snapshots, the porous media are drawn with transparent spheres, and the noncollapsed polymer is drawn with yellow beads.

it [Fig. 3(i)]. Nevertheless, thermal fluctuation can nucleate a protrusion that can then be dragged by the extensional flow at the pore throat to trigger the globule-stretch transition [Figs. 3(ii) and 3(iii)] [38,39]. The stretched polymer conformation then facilitates the polymer transport until reaching the next pore throat [Fig. 3(iv)].

Finally, in the reptation regime the noncollapsed polymers ($\varepsilon = 0.41$, $Pe = 15$ or 150) have a transport velocity $V/V_p \sim 0.8$ that is slower than the collapsed polymers ($\varepsilon = 2.08$, $Pe = 150$) with $V/V_p \sim 1$ [cf. Fig. 2(a)]. This difference is due to the formation of hooks for the noncollapsed polymers when passing through obstacles that slow down the polymer transport [40,41]. Figure 4 shows $\Delta R(t)/L$ and $R_g(t)/L$ for a noncollapsed polymer ($L_c/L = 3.33$) that passes through pore throats as well as representative simulation snapshots for the $\varepsilon = 0.41$, $Pe = 15$ case, which the hooking-unhooking dynamics can be clearly observed [Figs. 4(ii)–4(iv)]. Interestingly, due to the threefold symmetry of the fcc ⟨111⟩ direction we observe a "Y collision" with polymer strands concurrently pulled in three directions [Fig. 4(i)], which has not been discussed in prior literature [42,43] and may be worth further investigation.

In summary, we have presented hydrodynamic simulation results for polymers flowing through model porous media (fcc colloidal crystal) under different flow rates and solvent properties. The most prominent finding was the emergent of slow dynamics for collapsed polymers at low flow rate, where the transport velocity of polymers can be slowed down by as much as 5 times compared to the pore fluid velocity ($V/V_p \sim 0.2$). For using polymers for industrial subsurface applications, a retarding factor of 5 may result in huge delays for the project completion, and extra care should be taken to ensure the polymers are in the noncollapsed state in the subsurface environments to avoid any mechanical entrapment. Indeed, in this work we have mainly focused on the model porous media (colloidal crystal) with well-defined pore geometries. How the more complex porous media (e.g., sedimentary rocks such as sandstones and carbonates) with irregular pore geometries may affect the transport of polymers remains an interesting topic for future study. On the other hand, we have observed an extra window for size-dependent transport velocity ($1 \lesssim L_c/L \lesssim 2$) for the collapsed polymers in low flow rate. In the context of macromolecular separation, we may try to modulate the solvent properties (by mixing different solvents, changing temperatures and ionic strengths, etc.) to add an extra dimension to achieve further separation ranges and resolutions when flowing polymers through porous media such as gels or microfluidic devices.

We thank Aramco Research Center-Boston, Reservoir Engineering Technology team members for valuable discussions. We acknowledge ASC, IT Services for managing computational resources.

[1] J.-L. Viovy, Rev. Mod. Phys. **72**, 813 (2000).
[2] K. D. Dorfman, Rev. Mod. Phys. **82**, 2903 (2010).
[3] K. D. Dorfman, S. B. King, D. W. Olson, J. D. Thomas, and D. R. Tree, Chem. Rev. **113**, 2584 (2013).
[4] L. W. Lake, *Enhanced Oil Recovery* (Prentice Hall, Englewood Cliffs, NJ, 1989).
[5] M. M. Smith, J. A. Silva, J. Munakata-Marr, and J. E. McCray, Environ. Sci. Technol. **42**, 9296 (2008).
[6] R. Farajzadeh, P. Bedrikovetsky, M. Lotfollahi, and L. Lake, Water Resour. Res. **52**, 2279 (2016).
[7] S. Al-Hajri, S. M. Mahmood, H. Abdulelah, and S. Akbari, Energies **11**, 2751 (2018).
[8] M. Kawelah, Y. He, H. Alamri, A. Gizzatov, T. M. Swager, and S. S. Zhu, Energy Fuels **34**, 12018 (2020).
[9] D. Kawale, E. Marques, P. L. Zitha, M. T. Kreutzer, W. R. Rossen, and P. E. Boukany, Soft Matter **13**, 765 (2017).
[10] D. Kawale, G. Bouwman, S. Sachdev, P. L. Zitha, M. T. Kreutzer, W. R. Rossen, and P. E. Boukany, Soft Matter **13**, 8745 (2017).

[11] C. A. Browne, A. Shih, and S. S. Datta, Small **16**, 1903944 (2020).
[12] C. A. Browne, A. Shih, and S. S. Datta, J. Fluid Mech. **890** (2020).
[13] E. M. Ekanem, S. Berg, S. De, A. Fadili, T. Bultreys, M. Rücker, J. Southwick, J. Crawshaw, and P. F. Luckham, Phys. Rev. E **101**, 042605 (2020).
[14] E. O. I. Shaffer and M. Olvera de La Cruz, Macromolecules **22**, 1351 (1989).
[15] P. D. Patel and E. S. Shaqfeh, J. Chem. Phys. **118**, 2941 (2003).
[16] A. Mohan and P. S. Doyle, Phys. Rev. E **76**, 040903(R) (2007).
[17] N. Laachi and K. D. Dorfman, J. Chem. Phys. **133**, 234104 (2010).
[18] A. Alexander-Katz, M. F. Schneider, S. W. Schneider, A. Wixforth, and R. R. Netz, Phys. Rev. Lett. **97**, 138101 (2006).
[19] S. Schneider, S. Nuschele, A. Wixforth, C. Gorzelanny, A. Alexander-Katz, R. Netz, and M. F. Schneider, Proc. Natl. Acad. Sci., USA **104**, 7899 (2007).
[20] A. Alexander-Katz and R. Netz, Macromolecules **41**, 3363 (2008).
[21] A. Alexander-Katz, H. Wada, and R. R. Netz, Phys. Rev. Lett. **103**, 028102 (2009).
[22] A. Buguin and F. Brochard-Wyart, Macromolecules **29**, 4937 (1996).
[23] H. Chen, A. Z. Panagiotopoulos, and E. P. Giannelis, Langmuir **31**, 2407 (2015).
[24] H. Chen, J. R. Cox, H. Ow, and R. Shi, and A. Z. Panagiotopoulos, Sci. Rep. **6**, 28553 (2016).
[25] H. Chen and A. Alexander-Katz, Phys. Rev. Lett. **107**, 128301 (2011).
[26] H. Chen and A. Alexander-Katz, Phys. Rev. E **89**, 032602 (2014).
[27] M. Rubinstein and R. H. Colby, *Polymer Physics* (Oxford University Press, Oxford, 2003).
[28] B. Dünweg, U. D. Schiller, and A. J. C. Ladd, Phys. Rev. E **76**, 036704 (2007).
[29] S. Succi, *The Lattice Boltzmann Equation: For Fluid Dynamics and Beyond* (Oxford University Press, Oxford, 2001).
[30] H. Chen, Sc.D. thesis, Massachusetts Institute of Technology, 2013.
[31] P. Ahlrichs and B. Dünweg, J. Chem. Phys. **111**, 8225 (1999).
[32] A. J. C. Ladd, R. Kekre, and J. E. Butler, Phys. Rev. E **80**, 036704 (2009).
[33] H. Chen, M. A. Fallah, V. Huck, J. I. Angerer, A. J. Reininger, S. W. Schneider, M. F. Schneider, and A. Alexander-Katz, Nat. Commun. **4**, 1333 (2013).
[34] H. Chen and A. Alexander-Katz, Soft Matter **9**, 10381 (2013).
[35] E. Fattahi, C. Waluga, B. Wohlmuth, U. Rüde, M. Manhart, and R. Helmig, Comput. Fluids **140**, 247 (2016).
[36] M. R. Newton, K. A. Morey, Y. Zhang, R. J. Snow, M. Diwekar, J. Shi, and H. S. White, Nano Lett. **4**, 875 (2004).
[37] D. C. Rapaport, *The Art of Molecular Dynamics Simulation* (Cambridge University Press, Cambridge, 2004).
[38] C. E. Sing and A. Alexander-Katz, Macromolecules **43**, 3532 (2010).
[39] C. E. Sing and A. Alexander-Katz, Biophys. J. **98**, L35 (2010).
[40] D. C. Schwartz and M. Koval, Nature (London) **338**, 520 (1989).
[41] H. Zhang and M. J. Wirth, Anal. Chem. **77**, 1237 (2005).
[42] J. M. Kim and P. S. Doyle, Macromolecules **40**, 9151 (2007).
[43] T. Shendruk, O. Hickey, G. Slater, and J. Harden, Curr. Opin. Colloid Interface Sci. **17**, 74 (2012).